Published in final edited form as:
Structure. 2013 November 5; 21(11): . doi:10.1016/j.str.2013.08.026.

Structure of FGFR3 transmembrane domain dimer: implications for signaling and human pathologies

Eduard V. Bocharov[1,*], **Dmitry M. Lesovoy**[1], **Sergey A. Goncharuk**[1,2], **Marina V. Goncharuk**[1,2], **Kalina Hristova**[3], and **Alexander S. Arseniev**[1,4]

[1]Department of Structural Biology, Shemyakin–Ovchinnikov Institute of Bioorganic Chemistry RAS, str. Miklukho-Maklaya 16/10, Moscow, 117997, Russian Federation

[2]Department of Bioengineering, Faculty of Biology, Lomonosov Moscow State University, Leninskie gori 1, Moscow, 119234, Russian Federation

[3]Department of Materials Science and Engineering, Johns Hopkins University, Baltimore, MD 21218, USA

[4]Moscow Institute of Physics and Technology (State University), Institutskiy Pereulok 9, Dolgoprudny, Moscow region, 141700, Russian Federation

SUMMARY

Fibroblast growth factor receptor 3 (FGFR3) transduces biochemical signals *via* lateral dimerization in the plasma membrane, and plays an important role in human development and disease. At least 8 different pathogenic mutations, implicated in cancers and growth disorders, have been identified in FGFR3 transmembrane segment. Here we use heteronuclear NMR spectroscopy to determine the dimeric structure of FGFR3 transmembrane domain in membrane-mimicking DPC/SDS (9/1) micelles. In the structure, the two transmembrane helices pack into a symmetric left-handed dimer, with intermolecular stacking interactions occurring in the dimer central region. Some pathogenic mutations fall within the helix-helix interface, while others are located within a putative alternative interface. This implies that while the observed dimer structure is important for FGFR3 signaling, the mechanism of FGFR3-mediated transduction across the plasma membrane is complex. We propose a FGFR3 signaling mechanism that is based on the solved structure, available structures of isolated soluble FGFR domains, and published biochemical and biophysical data.

INTRODUCTION

The four human fibroblast growth factor receptors (FGFRs) belong to the family of receptor tyrosine kinases (RTKs) and transduce diverse biochemical signals by lateral dimerization in the plasma membrane, followed by receptor autophosphorylation and stimulation of downstream signaling cascades (Mohammadi et al al., 2005; Lemmon and Schlessinger, 2010). These bitopic membrane proteins consist of an extracellular (EC) domain with three

[*]Correspondence may be addressed to: Dept. of Structural Biology, IBCh RAS, Str. Miklukho-Maklaya, 16/10, Moscow, Russian Federation, 117997; Tel.: +7(495)330-74-83; Fax: +7(495)335-50-33; bon@nmr.ru (E.V.B.).

SUPPLEMENTAL INFORMATION

Supplemental information includes eleven figures and two tables and can be found with this article at doi: 10.1016/j.str

immunoglobulin-like (D1, D2, D3) subdomains, a single-span transmembrane (TM) domain, and a cytoplasmic component with tyrosine kinase activity. The kinase domain exhibits a typical bilobal fold, consisting of an N-terminal lobe that acts as an enzyme and a C-terminal lobe that acts as a substrate (Mohammadi et al al., 2005; Bae and Schlessinger, 2010). Specific ligands (fibroblast growth factors) and heparin/heparan sulfate proteoglycans bind to the D2-D3 subdomains of FGFR, thus stabilizing the dimeric complex and enhancing its activity. The D1 subdomain engages in weak interactions with the D2-D3 subdomains, which are sufficient for sustainable autoinhibition (Mohammadi et al al., 2005).

FGFRs play an important role in human growth and development, and in the adult. Mutations in these membrane proteins result in various disorders of the connective tissues and the skeleton. Among the family, FGFR3 is known for the largest number of pathogenic mutations observed in human (Passos-Bueno et al., 1999; Li and Hristova, 2006). The most frequent pathogenic mutations G380R and A391E in the TM region of FGFR3 are associated both with cancer and with disorders in skeletal development, causing achondropalsia and Crouzon syndrome with acanthosis nigricans, respectively. The exact mechanism of FGFR3-mediated signal transduction in health and disease is unknown, and likely will not emerge until high-resolution structures of full-length wild-type and mutant FGFR3 dimers in various stages of their activation become available. While obtaining structures of full-size RTK proteins is still not feasible, isolated soluble RTK domains have been produced and studied. In particular, crystal structures have been obtained for the EC ligand-binding domains as well as for the kinase domains of FGFRs in different functional states (Bae and Schlessinger, 2010; Mohammadi et al., 2005). To complete the picture, in the present paper we describe the high-resolution NMR structure of the human FGFR3 TM domain dimer in a membrane-mimicking environment consisting of mixed DPC/SDS (9/1) micelles. The obtained structural-dynamic information along with the available biophysical and biochemical data provides useful insights into FGFR3 function at the molecular level.

RESULTS

FGFR3 TM helix undergoes a slow monomer-dimer transition in the micellar environment and elongates upon dimer formation

In order to investigate the structural and dynamic behavior of the TM domain of FGFR3 we prepared a recombinant 43-residue fragment $FGFR3_{357\text{-}399}$ (named FGFR3tm), which included the TM domain (residues Val^{372}-Leu^{398}) and the EC juxtamembrane (JM) region (residues Ala^{359}-Ser^{371} between the EC and TM domains). The self-association and monomer-dimer transition were detected for FGFR3tm embedded into mixed DPC/SDS (9/1) micelles at detergent/peptide molar ratios (D/P) lower than 120 (Figure 1; see also Figure S1A in Supplemental information available online). This was confirmed by the analysis of ^{15}N,^{13}C-F1-filtered/F3-edited-NOESY spectrum acquired at D/P of 65 that reveals the characteristic NOE connectivities for a dimeric structure of FGFR3tm (Figure 1C; see also Table S1 and Figure S2). As the minimal distinguishable chemical shift difference between signals of two states in the $^{1}H/^{15}N$-TROSY spectrum is ~20 Hz, the monomer-dimer transition is a slow process (on the millisecond timescale or slower) with an occupancy of the states and apparent free energy of association ΔG_{app} dependent on D/P (Figure S1). At lower D/P values, the dimer population increases rapidly, but this is accompanied by the appearance of an additional broad satellite signal near some amide cross-peaks in the NMR spectra (Figure 1B), indicative of higher-order oligomerization, followed by sample precipitation.

Since only one set of signals can be seen in the NMR spectra for FGFR3tm in the dimeric state, the dimer is symmetrical on the NMR timescale (in the millisecond range). Therefore, the distance and torsion angle restraints identified for FGFR3tm were symmetrized in order

to obtain the dimer spatial structure (Table 1 and Figure 2A; see also Figure S4). The relatively long (~43 Å) TM helix of the FGFR3tm dimer subunit consists of a water-exposed N-terminal turn 369-371 followed by stable 3_{10}- and α-helical TM regions 372–378 and 379–398, respectively (Figure 2B; see also Figures S3, S4 and S5). In the helical regions, besides backbone hydrogen-bonding, the side-chain hydroxyl OγH groups of Ser^{378} and Thr^{394} form (according to local NOE pattern) intra-molecular hydrogen bonds with the backbone carbonyl groups of Gly^{375} and Val^{390}, respectively (Figure S6). The similar chemical shifts of ^{1}H, ^{13}C and ^{15}N nuclei for monomeric and dimeric forms of FGFR3tm indicate that the overall structure of the dimer subunits does not undergo significant changes upon helix-helix interaction. Nevertheless, in the monomeric state the N-terminal turn 369–372 of the TM helix is flexible and unfolded whereas its conformation is stabilized upon dimerization as revealed by the appearance of intra- (*i*, *i*+3) and inter-monomeric NOE connectivities with Ala^{369} (Figure 1C; see also Figure S7). Indeed, observed positive values of the differences between dimeric and monomeric $^{1}H^{N}$ chemical shifts in this region (Figure S4F) indicate a hydrogen bond formation (or stabilization) of the amide groups of Val^{372} and Tyr^{373} with adjacent potential acceptor groups (backbone carbonyl groups of Glu^{368}, Ala^{369}, or Gly^{370}). Moreover, in the dimeric state the short 3_{10}-helical region also becomes more rigid and/or changes its orientation relative to the α-helical part, which is reflected in a more pronounced rise, as compared to the C-terminal residues, in the local effective rotation correlation times τ_R along this region upon dimerization (Figure S4E). At the same time, the water-exposed and negatively charged N-terminal JM region 357–368 remains highly flexible.

The association mode of FGFR3 TM helices is mediated by a left-handed symmetric dimer *via* elongated heptad motif

In the micellar environment, the FGFR3tm TM helices $(Ala^{369}\text{-}Leu^{398})_2$ associate in a parallel fashion in a left-handed dimer *via* an extended heptad (Moore et al., 2008) motif $YA^{374}X_2L^{377}X_2G^{380}X_2FF^{384}X_2IL^{388}X_2A^{391}X_2TL^{395}$ with a distance *d* between the helix axes of 8.6 Å and a helix-helix crossing angle θ of 23° (Figure 2B, C). Along the heptad motif, a packing in the "knobs-into-holes" manner is mediated by van-der-Waals contacts of the large hydrophobic side-chains of valine, isoleucine and leucine residues, which are abundant on the large helix-helix contact surface extending over 870 $Å^2$. In the N-terminal part of the FGFR3tm dimer, the aromatic rings of opposite Tyr^{373} residues act, most likely, as anchors positioning the TM domain in the detergent headgroup region. The tight helix-helix packing in the central region of the FGFR3tm dimer is supported by intra- and inter-monomeric stacking π-π interactions of residues $(Y^{379}–FF^{384}–F^{386})_2$ forming an aromatic ring patch. The aromatic ring of Phe^{384} from one dimer subunit intercalates like a clasp between the rings of Tyr^{379} and Phe^{383} (involved in multiple inter-monomeric NOE contacts) of the second subunit. Indeed, the resonance broadening related to intermediate exchange processes (which occur with dimerization and are pronounced for the aromatic rings (Figure S8)) can be attributed, at least partially, to a change in mobility of the intercalating rings due to restriction of their flip-flop rotation (Wagner et al, 1976). In addition, weak polar inter-monomeric interactions between the Phe^{384} aromatic rings and the backbone atoms of the opposite Gly^{380} residues located near the point of closest helix approach also occur, supporting the observation that the dimerization is enhanced by the proximity of phenylalanine and glycine residues (Unterreitmeier et al., 2007). Thus, the FGFR3tm dimer is stabilized by multiple van-der-Waals and π-π contacts as well as weak electrostatic interactions. On the other hand, the charged residues flanking the TM helix on both termini have apparently profound destabilizing effect on the dimer. As was shown recently, FGFR3 TM helix association can be drastically amplified by amino acid substitutions in the C-terminal Arg patch ($CRLR^{399}$) (Peng et al., 2009). It should be noted that the standard free energy ΔG_o (Fleming, 2002) of FGFR3 TM helix association is rather

small in the used micellar environment (−1.3 kcal/mol, see Figure S1B) as well as in lipid bilayers (about −3 kcal/mol), which is typical for RTK TM domains (Li and Hristova, 2010; Bocharov et al., 2012). Noteworthy, such weak interactions may be critical for FGFR3 signaling, allowing the propagation of conformational changes in the dimer upon ligand binding.

DISCUSSION

A mechanistic model of FGFR3 signaling

It has been proposed that ligand binding increases FGFR activation by stabilizing the receptor dimer and/or altering the preformed dimer structure (Belov and Mohammadi, 2012). Unliganded FGFR dimers are phosphorylated to a small degree, which is often referred to as “basal” phosphorylation level; this results in basal “noise” activity. Upon ligand binding, the FGFR dimer moves into a state with higher phosphorylation level and full activity. The dimeric adaptor protein Grb2 can inhibit the basal activity of FGFR (and, seemingly, of other RTKs) by means of entrapping the otherwise mobile kinase domain C-termini of the preformed receptor dimer in a partially phosphorylated state (when only tyrosines in the activation loop are phosphorylated) allowing rapid response to ligand stimulation (Belov and Mohammadi, 2012; Lin et al., 2012).

Here we present a spatial structure of FGFR3 TM domain dimer in a membrane-mimicking environment. There is also a high resolution structure of the monomeric EC domain of FGFR3 in the presence of a ligand (Mohammadi et al., 2005). However, no high resolution structures of FGFR3 kinase domain are available to date. On the other hand, the monomeric and dimeric structures of EC and kinase domains have been described for different functional states of FGFR1 and FGFR2, as well as of receptors from other RTK families (Bae and Schlessinger, 2010; Mohammadi et al., 2005). As there are no structures of full-length RTKs, we do not fully understand how different domains function together to mediate signal transduction inside the cell. Nevertheless, the available structures of isolated RTK domains have already greatly enhanced our understanding of RTK signaling.

Recent work has suggested that the asymmetry of RTK kinase domain dimers is likely a critical determinant of their activity. The discoveries that (i) EGFR kinases are activated allosterically upon the formation of asymmetric kinase dimers and that (ii) inactive EGFR kinase dimers are likely symmetric have spurred investigations of the role of structural asymmetry in the activation of other RTKs (Lemmon and Schlessinger, 2010; Jura et al., 2009; Landau and Ben-Tal, 2008). The kinase domains of FGFR also form an asymmetric dimer during receptor activation, whereas the symmetric kinase dimer is attributed to an autoinhibited conformation (Mohammadi et al., 1996; Bae and Schlessinger, 2010). Asymmetric kinase domain dimers have been reported for FGFR1 and FGFR2, with structures that are distinctly different from the structure of the asymmetric EGFR kinase domain dimer (Bae and Schlessinger, 2010). This is not surprising, as FGFR kinases are activated *via* cross-phosphorylation of tyrosines on the activation loop and not allosterically like EGFR (Lemmon and Schlessinger, 2010). Yet, the very discovery of FGFR kinase domain asymmetric dimers suggests that the role of symmetry in the activation control may be similar throughout the RTK family. By analogy with EGFR, it can be hypothesized that the asymmetric FGFR kinase dimers are fully active and that symmetric kinase dimers exist in the basal phosphorylation state. If two distinct FGFR3 dimeric structures exist, does the solved TM dimer structure correspond to the basal phosphorylation state, or to the high activity state? For the EGFR dimers, it has been argued that the C-termini of the TM domains need to be spaced apart (by about 20 Å) in order for the asymmetric kinase dimer configuration to be achieved (Jura et al., 2009). As the helices in the observed FGFR3 TM structure are packed *via* an extended heptad motif with a small crossing angle between the

helices, the C-termini are very close and, therefore, one can hypothesize that the structure corresponds to the basal phosphorylation state.

On the other hand, an extended concavity covers the N-terminal half of the FGFR3 TM helix, with Gly, Ser and Ala residues creating a weakly polar surface outside of the observed dimerization interface (Figure 2C). These residues with small side-chains are parts of small-X_3-small tetrad motifs $G^{370}X_3A^{374}X_3S^{378}X_3G^{382}$ and $S^{371}X_3G^{375}$. These so-called GG4-like motifs have been shown to mediate dimerization in many membrane proteins, including RTKs (Moore et al., 2008; Bocharov et al., 2008; Bocharov et al., 2010a). It is therefore possible that an alternative FGFR3 TM dimer structure, employing the GG4-like motifs, exists. Such a putative structure can be expected to have helix-helix crossing angle near 40° (Moore et al., 2008; Bocharov et al., 2010a) and can be obtained from the experimentally observed conformation through rotation of the TM helices around their axes followed by a helix-helix crossing angle increase. As the site of the expected contact is close to the N-terminus and the crossing angle is large, the C-termini of the TM helices will be more spaced in this dimer structure than in the observed dimerization mode. We can thus hypothesize that this alternative dimerization mode *via* the N-terminal GG4-like motifs (Figure 2C) corresponds to the fully active FGFR3 state (similarly to EGFR kinase activation model (Jura et al., 2009)).

The conformation of the unliganded RTK EC domains likely prevents the transition to the fully active dimer state (Endres et al., 2013). Indeed, FGFR3 EC domain has been found to inhibit dimerization (by ~1 kcal/mol) in the absence of ligand, while the TM domain interaction has been shown to stabilize the FGFR3 dimer (by ~−4 kcal/mol) (Li and Hristova, 2010; Chen et al., 2010). Based on the above arguments, we propose that the FGFR3 unliganded dimer is stabilized by the heptad motif contacts shown in Figure 2C, in addition to possible stabilization due to kinase domain and Grb2 interactions. Upon ligand binding, there are conformational changes in the FGFR3 EC domains that stabilize the EC domain dimer. The liganded FGFR3 EC domain dimer likely adopts the symmetric conformation observed in the crystal structures of the isolated FGFR1 D2-D3 subdomains in the presence of fgf and heparin (Mohammadi et al., 2005). We propose that upon ligand binding, the full-length FGFR3 dimer undergoes a further conformational transition, in the course of which the TM domain dimer switches into the alternative structure mediated by the N-terminal GG4-like motifs. As there is a “hard linkage” between the TM domain and the kinase domain (Bell et al., 2000), the rearrangements within the TM dimer, which increase the distance between the TM domain C-termini, likely allow for the transition to the asymmetric fully active kinase conformation.

What mechanism can underlie the TM dimer interface switch in response to ligand binding? Remarkably, according to the crystal structures, the C-termini of the ligand-bound EC domains in the activated FGFR dimer are spaced apart by at least ~50 Å (Mohammadi et al., 2005). On the other hand, the flexible extracellular JM regions (about ten residues each, with a total length of ~30 Å in the fully extended conformation) have to bridge the C-termini of the EC domains and the N-termini of the TM helices, which are close to each other in both dimerization modes. So, ligand binding to the preformed FGFR dimer would cause unwinding of the extracellular JM regions, creating tension in the receptor structure. In order to meet these restraints, changes of the secondary structure of each TM helix (e.g., unfolding of the N-terminal turn $A^{369}GSV^{372}$) as well as rotational rearrangements of the TM dimer subunits with respect to each other, are likely required, thus inducing transition to the alternative dimerization mode. The increase of the helix-helix crossing angle resulting in a large separation between the C-termini of the TM helices would provide adequate space for proper asymmetric orientation of the kinase domains, followed by Grb2 release allowing further receptor autophosphorylation and downstream signaling cascades. Thus, the kinase

domains follow the structural rotational rearrangements of the TM helices, as has been demonstrated for the Neu and EGF receptors (Bell et al., 2000; Moriki et al., 2001). This mechanism is reminiscent of the movement of a marionette controlled by a puppeteer using strings (Figure 3). The ligand plays the role of the puppeteer and the short JM segments connecting the EC domains and TM helices behave as the strings, rotating the TM helices and providing the space required for an asymmetric disposition of the two kinase domains. Ligand binding has long been believed to stabilize the FGFR dimeric state, and even induce dimerization. In the model that we propose here, the role of the ligand is to create tension in EC domains and thus destabilize the symmetric kinase dimer, resulting in a transition to the asymmetric active kinase conformation.

FGFR3 TM domain dimerization alternatives and pathogenic mutations

The essential and diverse roles of RTKs are evident from the various developmental abnormalities and cancers that occur due to gain-of-function RTK signaling (Li and Hristova, 2006). Many of these mutations are believed to increase the population of fully active dimers in the plasma membrane (He and Hristova, 2012). Other consequences of the mutations may include processing defects, such as impeded trafficking and defective down-regulation (Cho et al., 2004; Bonaventure et al., 2007). A number of inherited skeletal malformations and cancers are caused by point mutations in FGFR3 TM domain (Li and Hristova, 2006). The right panel of Figure 2C (see also Table S2 and Figure S10) shows the mapping of known pathogenic mutations on the surface of the FGFR3 TM helix. Obviously, some pathogenic mutations, including the most common substitutions G380R and A391E causing the achondroplasia and Crouzon syndrome, fall within the observed TM helix-helix interface. This finding implies that the obtained TM dimer conformation is important for receptor functioning (at least for stabilizing the FGFR3 dimer in its basal phosphorylation state). Nevertheless, it would be difficult to envision that a single TM dimer structure can explain how all these mutations affect FGFR3 dimer structure and activity. The hypothesis that FGFR3 TM domain can form two alternative dimers, corresponding to the fully active and the basal phosphorylation states of the receptor, can provide the basis for such an explanations. In general, pathogenic mutations in the TM domain can either stabilize the fully active receptor conformation (e.g. by intermolecular hydrogen or S-S bonding), or destabilize the basal phosphorylation conformation (e.g. by imposing steric clashes or due to intra-membrane Coulomb repulsion of charged side-chains) and thus force the receptor into the fully active state (for more detailed discussion see subsection “Mechanistic insights into the effects of TM pathogenic mutations on FGFR3 helix-helix interactions” and Figure S11 in Supplemental information). This simple mechanistic interpretation can explain many experimental observations but has to be confirmed by structural studies of the corresponding pathogenic mutants. Finally, it should be kept in mind that other membrane proteins and the membrane environment can modulate the effect of the mutations and contribute to the diverse pathological phenotypes.

EXPERIMENTAL PROCEDURES

The ^{15}N- and ^{15}N/^{13}C-labeled and unlabeled sample of the recombinant peptide FGFR3tm (L^{357}PAEEELVEADEAGSVYAGILSYGVGFFLFILVVAAVTLCRLR^{399}) were produced in *Escherichia coli* and solubilized in an aqueous suspension of mixed d_{38}-dodecylphosphocholine/ d_{29}-sodiumdodecylsulfate (DPC/SDS = 9/1, mol/mol) micelles at pH 5.7 according to (Goncharuk et al., 2011). Two NMR samples of FGFR3tm were prepared: a uniformly ^{15}N-labeled sample and a 1:1 mixture of unlabeled and ^{15}N/^{13}C-labeled peptide (referred to as “isotopic heterodimer” sample). The self-association of FGFR3tm was studied while varying the detergent/peptide molar ratio (D/P) within the range of 30 to 520. For the dimeric FGFR3tm structure determination, the concentrations of

the ^{15}N-labeled and "isotopic heterodimer" samples were 1.0 mM and 1.5 mM, respectively, at D/P of 65. NMR spectra were acquired at 40°C on 600 and 800 MHz AVANCE III spectrometers (Bruker BioSpin, Germany) equipped with pulsed-field gradient triple-resonance cryoprobes. ^{1}H, ^{13}C, and ^{15}N resonances of FGFR3tm were assigned with the CARA software (Keller, 2004) using two- and three-dimensional heteronuclear experiments (Cavanagh et al., 2006): ^{1}H/^{15}N-HSQC, ^{1}H/^{15}N-TROSY, ^{1}H/^{13}C-HSQC, ^{1}H/^{15}N-HNHA, ^{1}H/^{15}N-HNHB, ^{1}H/^{13}C/^{15}N-HNCA, ^{1}H/^{13}C/^{15}N-HN(CO)CA, ^{1}H/^{13}C/^{15}N-HNCO, ^{1}H/^{13}C-HCCH-TOCSY, ^{13}C- and ^{15}N-edited NOESY-HSQC/TROSY. The intra- and inter-monomeric NOE distance restraints were derived through the analysis of three-dimensional ^{15}N- and ^{13}C-edited NOESY and ^{15}N,^{13}C-F1-filtered/F3-edited-NOESY spectra (Stuart et al., 1999) acquired for the "isotopic-heterodimer" FGFR3tm sample. The spatial structure of the FGFR3tm dimer was calculated with the CYANA program (Güntert, 2003) based on proton-proton NOE connectivities and torsion angle restraints. The detailed experimental procedures of sample preparation and spatial structure calculation are described in Supplemental information. The atomic coordinates and structure factors of the FGFR3tm dimer have been deposited in the Protein Data Bank [PDB] (http://www.rcsb.org/) under accession ID code: 2LZL. The chemical shift assignments have been deposited in the Biological Magnetic Resonance Data Bank [BMRB] (www.bmrb.wisc.edu) under accession ID code: 18763.

Supplementary Material

Refer to Web version on PubMed Central for supplementary material.

Acknowledgments

The authors express their sincere thanks to Drs. P.E. Volynsky and K.V. Pavlov for helpful discussions. This work was supported by RAS Program "Molecular and Cellular Biology", RFBR (12-04-01816-a and 14-04-31947 mol_a) and U.S. NIH (GM068619) grants. Bocharov E.V. thanks personally Beirit K.A. ("Russian Funds" IG) for financial support.

References

Bae JH, Schlessinger J. Asymmetric tyrosine kinase arrangements in activation or autophosphorylation of receptor tyrosine kinases. Mol Cells. 2010; 29:443–448. [PubMed: 20432069]

Bell CA, Tynan JA, Hart KC, Meyer AN, Robertson SC, Donoghue DJ. Rotational coupling of the transmembrane and kinase domains of the Neu receptor tyrosine kinase. Mol Biol Cell. 2000; 11:3589–3599. [PubMed: 11029057]

Belov AA, Mohammadi M. Grb2, a double-edged sword of receptor tyrosine kinase signaling. Sci Signal. 2012; 5:pe49. [PubMed: 23131845]

Berjanskii MV, Neal S, Wishart DS. PREDITOR: a web server for predicting protein torsion angle restraints. Nucleic Acids Res. 2006; 34:W63–69. [PubMed: 16845087]

Bocharov EV, Mayzel ML, Volynsky PE, Mineev KS, Tkach EN, Ermolyuk YS, Schulga AA, Efremov RG, Arseniev AS. Left-handed dimer of EphA2 transmembrane domain: helix packing diversity among receptor tyrosine kinases. Biophys J. 2010b; 98:881–889. [PubMed: 20197042]

Bocharov EV, Mineev KS, Goncharuk MV, Arseniev AS. Structural and thermodynamic insight into the process of "weak" dimerization of the ErbB4 transmembrane domain by solution NMR. Biochim Biophys Acta. 2012; 1818:2158–2170. [PubMed: 22579757]

Bocharov EV, Mineev KS, Volynsky PE, Ermolyuk YaS, Tkach EN, Sobol AG, Chupin VV, Kirpichnikov MP, Efremov RG, Arseniev AS. Spatial structure of the dimeric transmembrane domain of the growth factor receptor ErbB2 presumably corresponding to the receptor active state. J Biol Chem. 2008; 283:6950–6956. [PubMed: 18178548]

Bocharov EV, Volynsky PE, Pavlov KV, Efremov RG, Arseniev AS. Structure elucidation of dimeric transmembrane domains of bitopic proteins. Cell Adh Migr. 2010a; 4:284–298. [PubMed: 20421711]

Bonaventure J, Horne WC, Baron R. The localization of FGFR3 mutations causing thanatophoric dysplasia type I differentially affects phosphorylation, processing and ubiquitylation of the receptor. Febs Journal. 2007; 274:3078–3093. [PubMed: 17509076]

Cavanagh, J.; Fairbrother, WJ.; Palmer, AG.; Skelton, NJ. Protein NMR spectroscopy: principles and practice. 2. Academic Press; San Diego, CA, USA: 2006.

Chen L, Placone J, Novicky L, Hristova K. The extracellular domain of fibroblast growth factor receptor 3 inhibits ligand-independent dimerization. Sci Signal. 2010; 3:ra86. [PubMed: 21119106]

Cho JY, Guo C, Torello M, Lunstrum GP, Iwata T, Deng C, Horton WA. Defective lysosomal targeting of activated fibroblast growth factor receptor 3 in achondroplasia. Proc Natl Acad Sci USA. 2004; 101:609–614. [PubMed: 14699054]

Endres NF, Das R, Smith AW, Arkhipov A, Kovacs E, Huang Y, Pelton JG, Shan Y, Shaw DE, Wemmer DE, Groves JT, Kuriyan J. Conformational Coupling across the Plasma Membrane in Activation of the EGF Receptor. Cell. 2013; 152:557–569. [PubMed: 23374350]

Fleming KG. Standardizing the free energy change of transmembrane helix–helix interactions. J Mol Biol. 2002; 323:563–571. [PubMed: 12381309]

Goncharuk SA, Goncharuk MV, Mayzel ML, Lesovoy DM, Chupin VV, Bocharov EV, Arseniev AS, Kirpichnikov MP. Bacterial synthesis and purification of transmembrane segment of the human FGFR3 receptor tyrosine kinase of wild type and mutant forms. Acta Naturae. 2011; 3:80–87.

Güntert P. Automated NMR protein structure calculation. Prog Nucl Magn Reson Spectrosc. 2003; 43:105–125.

He L, Hristova K. Physical-chemical principles underlying RTK activation and their implications for human disease. Biochim Biophys Acta. 2012; 1818:995–1005. [PubMed: 21840295]

Jura N, Endres NF, Engel K, Deindl S, Das R, Lamers MH, Wemmer DE, Zhang X, Kuriyan J. Mechanism for activation of the EGF receptor catalytic domain by the juxtamembrane segment. Cell. 2009; 137:1293–1307. [PubMed: 19563760]

Keller, RLJ. The Computer Aided Resonance Assignment Tutorial. CANTINA Verlag; Goldau, Switzerland: 2004.

Landau M, Ben-Tal N. Dynamic equilibrium between multiple active and inactive conformations explains regulation and oncogenic mutations in ErbB receptors. Biochim Biophys Acta. 2008; 1785:12–31. [PubMed: 18031935]

Lemmon MA, Schlessinger J. Cell signaling by receptor tyrosine kinases. Cell. 2010; 141:1117–1134. [PubMed: 20602996]

Li E, Hristova K. Role of receptor tyrosine kinase transmembrane domains in cell signaling and human pathologies. Biochemistry. 2006; 45:6241–6251. [PubMed: 16700535]

Li E, Hristova K. Receptor tyrosine kinase transmembrane domains: Function, dimer structure and dimerization energetics. Cell Adh Migr. 2010; 4:249–254. [PubMed: 20168077]

Li E, You M, Hristova K. FGFR3 dimer stabilization due to a single amino acid pathogenic mutation. J Mol Biol. 2006; 356:600–612. [PubMed: 16384584]

Lin CC, Melo FA, Ghosh R, Suen KM, Stagg LJ, Kirkpatrick J, Arold ST, Ahmed Z, Ladbury JE. Inhibition of Basal FGF Receptor Signaling by Dimeric Grb2. Cell. 2012; 149:1514–1524. [PubMed: 22726438]

Mohammadi M, Olsen SK, Ibrahimi OA. Structural basis for fibroblast growth factor receptor activation. Cytokine Growth Factor Rev. 2005; 16:107–113. [PubMed: 15863029]

Mohammadi M, Schlessinger J, Hubbard SR. Structure of the FGF receptor tyrosine kinase domain reveals a novel autoinhibitory mechanism. Cell. 1996; 86:577–587. [PubMed: 8752212]

Moore DT, Berger BW, DeGrado WF. Protein-Protein Interactions in the Membrane: Sequence, Structural, and Biological Motifs. Structure. 2008; 16:991–1001. [PubMed: 18611372]

Moriki T, Maruyama H, Maruyama IN. Activation of preformed EGF receptor dimers by ligand-induced rotation of the transmembrane domain. J Mol Biol. 2001; 311:1011–1026. [PubMed: 11531336]

Passos-Bueno MR, Wilcox WR, Jabs EW, Sertie AL, Alonso LG, Kitoh H. Clinical spectrum of fibroblast growth factor receptor mutations. Hum Mutat. 1999; 14:115–125. [PubMed: 10425034]

Peng WC, Lin X, Torres J. The strong dimerization of the transmembrane domain of the fibroblast growth factor receptor (FGFR) is modulated by C-terminal juxtamembrane residues. Protein Sci. 2009; 18:450–459. [PubMed: 19165726]

Stuart AC, Borzilleri KA, Withka JM, Palmer AG III. Compensating for variations in $^{1}H–^{13}C$ scalar coupling constants in isotope-filtered NMR experiments. J Am Chem Soc. 1999; 121:5346–5347.

Unterreitmeier S, Fuchs A, Schäffler T, Heym RG, Frishman D, Langosch D. Phenylalanine promotes interaction of transmembrane domains *via* GxxxG motifs. J Mol Biol. 2007; 374:705–718. [PubMed: 17949750]

Volynsky PE, Polyansky AA, Fakhrutdinova GN, Bocharov EV, Efremov RG. Role of dimerization efficiency of transmembrane domains in activation of fibroblast growth factor receptor 3. J Am Chem Soc. 2013; 135:8105–8108.

Wagner G, DeMarco A, Wüthrich K. Dynamics of the aromatic amino acid residues in the globular conformation of the basic pancreatic trypsin inhibitor (BPTI). I ^{1}H NMR studies. Biophys Struct Mech. 1976; 23:139–158. [PubMed: 9165]

Highlights

1. FGFR3 TM domains associate in a left-handed parallel helical dimer *via* a heptad motif
2. The solved NMR structure likely corresponds to the FGFR3 basal phosphorylation state
3. Some, but not all, pathogenic mutations fall within the FGFR3 TM dimer interface
4. FGFR3 signaling mechanism based on two alternative TM dimerization modes is proposed

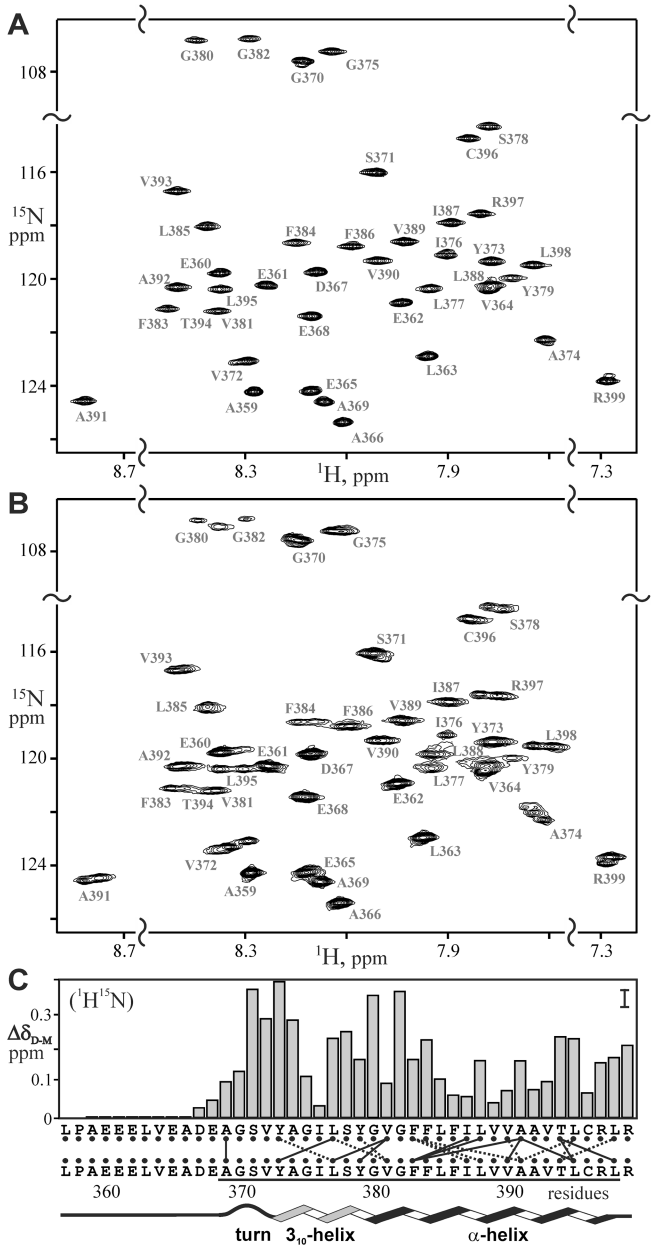

Figure 1. NMR spectra of FGFR3tm in a membrane-mimicking environment

Heteronuclear ^{1}H/^{15}N-TROSY NMR spectra of FGFR3tm in mixed DPC/SDS (9/1) micelles at D/P of 140 **(A)** and 65 **(B)**, 40 °C and pH 5.7. The ^{1}H-^{15}N backbone and side-chain resonance assignments are shown. The TM region 367-399 undergoes a slow monomer-dimer transition, as proved by the comparison of the ^{1}H/^{15}N-TROSY (appearance of signal doubling) and ^{15}N,^{13}C-F1-filtered/F3-edited-NOESY (registration of inter-monomeric NOE) spectra acquired at D/P of 140 and 65. **(C)** Generalized chemical shift changes, $\Delta\delta(^{1}H^{15}N)_{d\text{-}m}$, for the FGFR3tm amide groups are calculated as the geometrical distance (with weighting of ^{1}H shifts by a factor of 5 compared to ^{15}N shifts) between the amide cross-peaks assigned to the dimeric and monomeric FGFR3tm states in the ^{1}H-^{15}N TROSY spectrum acquired at D/P of 65. The measurement uncertainty is shown in the upper right corner. *Bottom*, pattern of unambiguous inter-monomeric NOE connectivities (shown

with *solid* and *dashed* lines), identified between the subunits (underlined) of the symmetric FGFR3tm dimer.

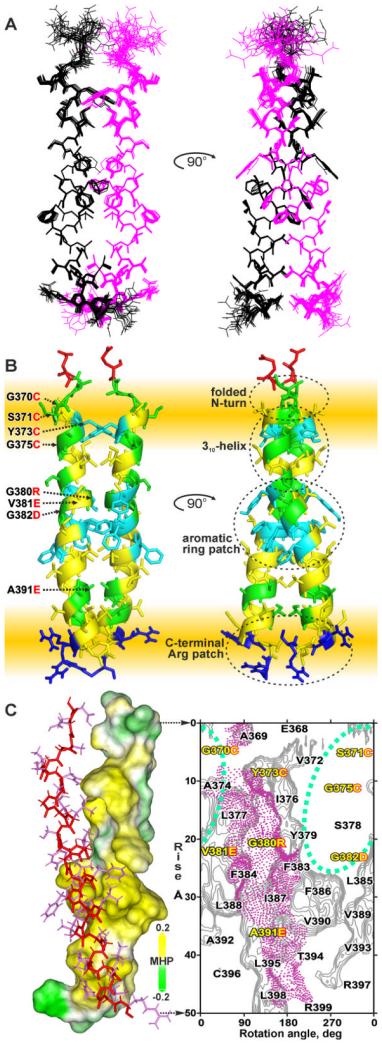

Figure 2. Spatial structure of the FGFR3tm dimer

(A) The 25 NMR structures of the FGFR3tm dimer are superimposed on backbone atoms of the TM helical regions $(Tyr^{373}\text{-}Leu^{398})_2$. Heavy atom bonds are shown only and painted in *black* and *magenta* for different dimer subunits. **(B)** Ribbon structure of the FGFR3tm dimer. The negative charged, positive charged, aromatic, large hydrophobic and small side-chains are shown in *red*, *blue*, *cyan*, *light yellow* and *green*, respectively. The approximate position of the membrane borders is highlighted by the *yellow* strips. Pathogenic mutations are shown by arrows. **(C)** Properties of the FGFR3tm dimer interface. *Left:* hydrophobic and hydrophilic (polar) surfaces of the TM helix subunit are colored in *yellow* and *green*, respectively. The complementary subunit is shown in a stick representation. *Right:* hydrophobicity map of the molecular surface of the TM helix with the isolines encircling hydrophobic regions with high molecular hydrophobicity potential (MHP) values. The map, constructed as described in Supplemental experimental procedures, is presented in cylindrical coordinates associated with the TM helix. The observed helix packing interface of FGFR3tm is indicated with *magenta* dots. An alternative dimerization interface, rich in consensus helix packing GG4-like motifs, is encircled by the *light green* oval. Noteworthy, similar dimerization interfaces were predicted for the FGFR3 TM domain by molecular modeling (Li et al., 2006; Volynsky et al., 2013). Residues which harbor pathogenic

mutations (Li and Hristova, 2006) are highlighted in *yellow* with amino acid substitution marked additionally in *red*.

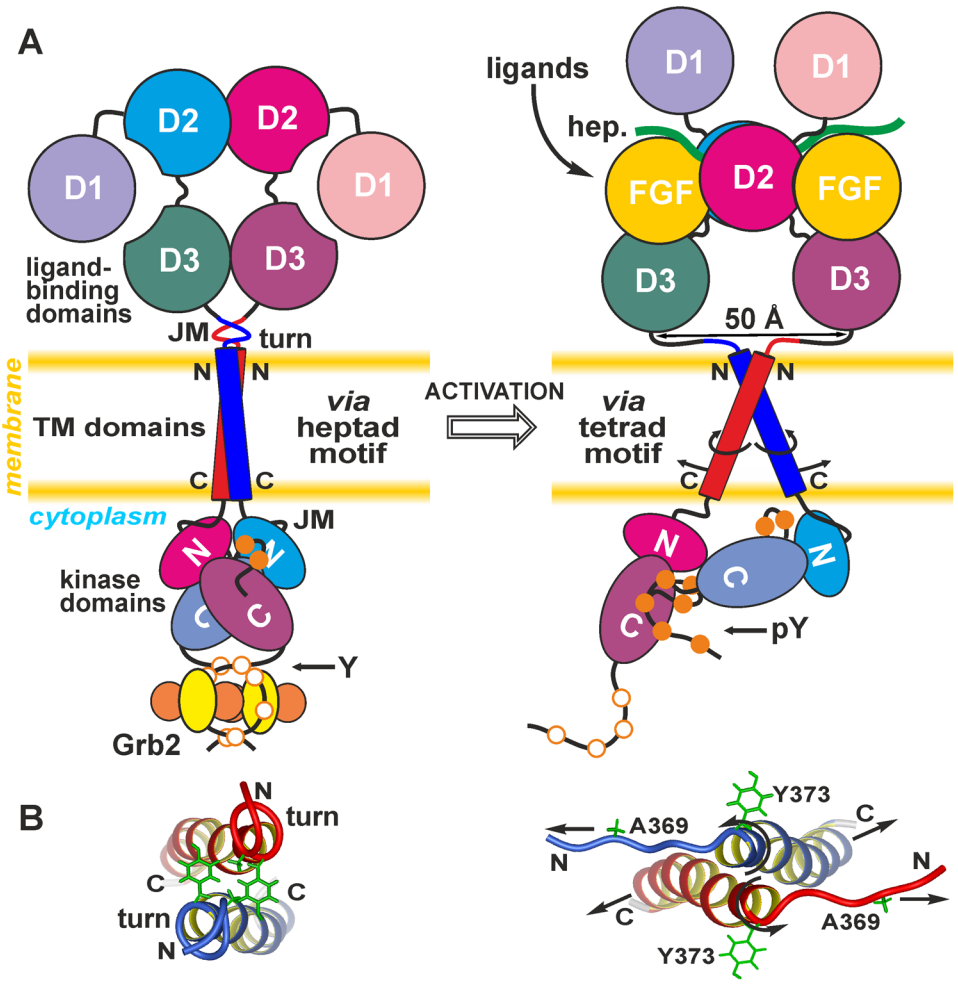

Figure 3. "String-puppet" mechanism of FGFR3 activation under the assumption that two alternative dimer structures exist in the presence and absence of ligand

(A) *Left:* The FGFR3 TM domain dimer is formed *via* the heptad motif shown in Figure 2. The small TM helix-helix crossing angle keeps the receptor cytoplasmic domains in a symmetric configuration, resulting in a basal phosphorylation state, which is stabilized by the homodimeric adaptor protein Grb2. The autophosphorylation sites are schematically presented by open and filled *orange* circles. The disposition of the EC domains in the unliganded FGFR3 dimer is not known. *Right:* FGFR3 activation requires asymmetric configuration of the kinase domains, which is easier to achieve when the C-termini of the TM FGFR3 domains are spaced apart (by ~20 Å). This configuration corresponds to an alternative dimerization mode of the TM domain, utilizing the N-terminal tetrad GG4-like motif. Ligand-binding (FGF and heparin/heparan) induces a conformational change in the EC domain and pushes the D3 subdomains (i.e. the C-termini of the EC domains) away from each other (by ~50 Å). This structural change imposes spatial restraints *via* the short extracellular JM regions ("strings") on the configuration of the entire receptor dimer, inducing motions in the receptor dimer, Grb2 release and receptor activation. The TM domain dimer switches into the high crossing angle structure, and the kinase domains adopt the fully active asymmetric configuration. **(B)** Schematic *top* view of the FGFR3 TM domain dimer in its putative basal phosphorylation (*left*) and fully active (*right*) conformations mediated by the heptad and tetrad motifs, respectively. Analogous TM helix

packing diversity was recently observed for other RTKs (Bocharov et al., 2010b), see also Figure S9. Ligand-binding followed by structural rearrangements of the EC domains and extension of the extracellular JM regions likely induces unfolding of the N-terminal turn $A^{369}GSV^{372}$ and rotational movements of the TM helices, which increases the distance between their C-termini and allows for the formation of the asymmetric kinase dimer.

Table 1

Structural statistics for the ensemble of 25 NMR structures of the FGFR3tm dimer (PDB ID: 2LZL)

NMR distance & dihedral restraints	
Total unambiguous NOE restraints	586
intra-residue	226
inter-residue	334
sequential (|i-j|=1)	174
medium-range (1<|i-j|≤4)	160
long-range (|i-j|>4)	0
inter-monomeric NOE	26
Hydrogen bond restraints (upper/lower)	
for 19×2 backbone to backbone	114/114
for 2×2 side-chain to backbone	8/8
Total torsion angle restraints	154
backbone φ	52
backbone ψ	52
side-chain χ^1	42
side-chain χ^2	10
Structure calculation statistics	
CYANA target function (Å^2)	1.5±0.1
Restraint violations	
distance (>0.2 Å, >0.25 Å)	2, 0
dihedral (>5°, >6°)	2, 0
Average pairwise r.m.s.d. (Å)	
stable TM helix region $(373–398)_2$	
backbone atoms	0.24±0.10
all heavy atoms	0.78±0.14
TM helix region $(369–398)_2$	
backbone atoms	0.27±0.12
all heavy atoms	0.73±0.18
Ramachandran analysis	
% residues in most favored regions	91.7
% residues in additional allowed regions	8.2
% residues in generously allowed regions	0.1
% residues in disallowed regions	0.0
Helix-helix packing	
Contact surface area per dimer subunit (Å^2)	870±40
Angle θ between the TM helix axes (deg.)	23±2
Distance d between the TM helix axes (Å)	8.6±0.4